The Astrophysical Journal, 991:133 (12pp), 2025 October 1 https://doi.org/10.3847/1538-4357/adfc72

Very Late-time JWST and Keck Spectra of the Oxygen-rich Supernova 1995N

Geoffrey C. Clayton[1,2,3], R. Wesson[4], Ori D. Fox[5], Melissa Shahbandeh[5,6], Alexei V. Filippenko[7], Bryony Nickson[5], Michael Engesser[5], Schuyler D. Van Dyk[8], WeiKang Zheng[7], Thomas G. Brink[7], Yi Yang[9], Tea Temim[10], Nathan Smith[11], Jennifer Andrews[12], Chris Ashall[13], Ilse De Looze[14], James M. Derkacy[5], Luc Dessart[15], Michael Dulude[5], Eli Dwek[16,17], Ryan J. Foley[18], Suvi Gezari[5], Sebastian Gomez[5], Shireen Gonzaga[5], Siva Indukuri[6], Jacob Jencson[19], Joel Johansson[20], Mansi Kasliwal[21], Zachary G. Lane[22], Ryan Lau[23], David Law[5], Anthony Marston[24], Dan Milisavljevic[25], Richard O'Steen[5], Justin Pierel[5], Armin Rest[5,6], Arkaprabha Sarangi[26], Matthew Siebert[5], Michael Skrutskie[27], Lou Strolger[5], Tamás Szalai[28,29], Samaporn Tinyanont[30], Qinan Wang[31], Brian Williams[32], Lin Xiao[33], and Szanna Zsíros[28,34]

[1] Space Science Institute, 4765 Walnut St., Suite B, Boulder, CO 80301, USA; gclayton@spacescience.org
[2] Department of Physics & Astronomy, Louisiana State University, Baton Rouge, LA 70803, USA
[3] Maria Mitchell Association, 4 Vestal St., Nantucket, MA 02554, USA
[4] School of Physics and Astronomy, Cardiff University, Queens Buildings, The Parade, Cardiff CF24 3AA, UK
[5] Space Telescope Science Institute, 3700 San Martin Dr., Baltimore, MD 21218, USA
[6] Department of Physics and Astronomy, Johns Hopkins University, 3400 North Charles St., Baltimore, MD 21218, USA
[7] Department of Astronomy, University of California, Berkeley, CA 94720-3411, USA
[8] Caltech/IPAC, Mailcode 100-22, Pasadena, CA 91125, USA
[9] Physics Department, Tsinghua University, Beijing 100084, People's Republic of China
[10] Department of Astrophysical Sciences, Princeton University, Princeton, NJ 08544, USA
[11] Steward Observatory, University of Arizona, 933 N. Cherry St., Tucson, AZ 85721, USA
[12] Gemini Observatory, 670 N. Aohoku Place, Hilo, HI 96720, USA
[13] Institute for Astronomy, University of Hawai'i at Manoa, 2680 Woodlawn Dr., Honolulu, HI 96822-1839, USA
[14] Sterrenkundig Observatorium, Ghent University, Krijgslaan 281-S9, 9000 Gent, Belgium
[15] Institut d'Astrophysique de Paris, CNRS-Sorbonne Université, 98bis boulevard Arago, F-75014 Paris, France
[16] Department of Astronomy, University of Maryland, College Park, MD 20742, USA
[17] Center for Research and Exploration in Space Science and Technology (CRESST), NASA/GSFC, Greenbelt, MD 20771, USA
[18] Department of Astronomy and Astrophysics, University of California, Santa Cruz, CA 95064, USA
[19] IPAC, Mail Code 100-22, Caltech, 1200 E. California Blvd., Pasadena, CA 91125, USA
[20] Oskar Klein Centre, Department of Physics, Stockholm University, AlbaNova, SE-10691 Stockholm, Sweden
[21] Cahill Center for Astrophysics, California Institute of Technology, 1200 E. California Blvd. Pasadena, CA 91125, USA
[22] School of Physical and Chemical Sciences—Te Kura Matu, University of Canterbury, Private Bag 4800, Christchurch 8140, New Zealand
[23] NSF's NOIRLab, 950 N. Cherry Ave., Tucson, AZ 85719, USA
[24] European Space Agency (ESA), ESAC, 28692 Villanueva de la Canada, Madrid, Spain
[25] Purdue University, Department of Physics and Astronomy, 525 Northwestern Ave., West Lafayette, IN 4790720, USA
[26] DARK, Niels Bohr Institute, University of Copenhagen, Jagtvej 128, 2200 Copenhagen, Denmark
[27] Department of Astronomy, University of Virginia, Charlottesville, VA 22904-4325, USA
[28] Department of Experimental Physics, Institute of Physics, University of Szeged, Dóm tér 9, 6720 Szeged, Hungary
[29] MTA-ELTE Lendület "Momentum" Milky Way Research Group, Szent Imre H. st. 112, 9700 Szombathely, Hungary
[30] National Astronomical Research Institute of Thailand (NARIT), Chiang Mai, 50180, Thailand
[31] Department of Physics and Kavli Institute for Astrophysics and Space Research, Massachusetts Institute of Technology, 77 Massachusetts Ave., Cambridge, MA 02139, USA
[32] Observational Cosmology Lab, NASA Goddard Space Flight Center, Code 665, Greenbelt, MD 20771, USA
[33] Department of Physics, College of Physical Sciences and Technology, Hebei University, Baoding 071002, People's Republic of China
[34] HUN-REN CSFK Konkoly Observatory, Konkoly Thege M. ut 15-17, Budapest, 1121, Hungary
Received 2025 May 1; revised 2025 August 14; accepted 2025 August 14; published 2025 September 23

Abstract

We present new JWST/MIRI Medium Resolution Spectroscopy and Keck spectra of SN 1995N obtained in 2022–2023, more than 10,000 days after the supernova (SN) explosion. These spectra are among the latest direct detections of a core-collapse SN, both through emission lines in the optical and thermal continuum from infrared (IR) dust emission. The new IR data show that dust heating from radiation produced by the ejecta interacting with circumstellar matter is still present but greatly reduced from when SN 1995N was observed by the Spitzer Space Telescope and WISE in 2009/2010 and 2018, when the dust mass was estimated to be 0.4 $M_{\odot}$. New radiative-transfer modeling suggests that the dust mass and grain size may have increased between 2010 and 2023. The new data can alternatively be well fit with a dust mass of 0.4 $M_{\odot}$ and a much reduced heating source luminosity. The new late-time spectra show unusually strong oxygen forbidden lines, stronger than the Hα emission. This indicates that SN 1995N may have exploded as a stripped-envelope SN, which then interacted with a massive H-rich circumstellar shell, changing it from intrinsically Type Ib/c to Type IIn. The late-time spectrum results when the reverse shock begins to excite the inner H-poor, O-rich ejecta. This change in the spectrum is rarely seen but marks the start of the transition from SN to SN remnant.

Unified Astronomy Thesaurus concepts: Type II supernovae (1731); Dust formation (2269); Late stellar evolution (911)

1. Introduction

Core-collapse supernovae (CCSNe) are likely a major contributor of dust in the high-redshift Universe. Submillimeter observations indicate that early galaxies may contain up to $10^8\,M_\odot$ of dust at redshift $z \geqslant 6$ (e.g., F. Bertoldi et al. 2003; E. Dwek et al. 2014; C. R. Choban et al. 2025). If true, the dust budget requires $\sim 1\,M_\odot$ of dust to form in each supernova (SN; (E. Dwek et al. 2007).

In the last two decades, many nearby CCSNe have been studied to determine how much dust these objects can produce. Most studies of the mass of dust associated with CCSNe have been 2–3 orders of magnitude too small (e.g., S. Zsíros et al. 2024, and references therein). However, more recent observations enabled by larger telescopes and new technologies are allowing us to reexamine this perspective. For example, mid-infrared (IR) observations revealed at least $0.3\,M_\odot$ of dust in supernova remnant (SNR) G54.1+0.3 (T. Temim et al. 2017), while observations in the far-IR with the Herschel Space Observatory found 0.4–$0.7\,M_\odot$ of cold dust ($\sim$20 K) in the ejecta of SN 1987A (M. Matsuura et al. 2011, 2015), 0.1–$0.6\,M_\odot$ in the Cas A SNR (M. J. Barlow et al. 2010; I. De Looze et al. 2017), and 0.02–$0.4\,M_\odot$ in the Crab Nebula SNR (H. L. Gomez et al. 2012; T. Temim & E. Dwek 2013; P. J. Owen & M. J. Barlow 2015). More recently, James Webb Space Telescope (JWST) Mid-Infrared Instrument (MIRI) imaging of the Type IIP SN 2004et and Medium Resolution Spectroscopy (MRS) of the Type IIn SN 2005ip uncovered one of the largest newly formed dust masses in an extragalactic SN besides SN 1987A (M. Shahbandeh et al. 2023, 2025).

There are two competing scenarios for how these large masses of dust might be formed. The first suggests that there is continuous dust formation in the ejecta so the dust mass can continue to increase for decades (C. Gall et al. 2014; R. Wesson et al. 2015), while the second posits that large amounts of dust form at early times hidden in dense clumps (E. Dwek & R. G. Arendt 2015; E. Dwek et al. 2019). The results for SN 2005ip also raise the possibility that the postshock dust environment in some interacting SNe might be most conducive to dust formation (M. Shahbandeh et al. 2025). Therefore, extremely late-time measurements of CCSN dust are valuable but also quite rare given the faint nature of SNe at late times.

SN 1995N was discovered on 1995 May 5 (UTC dates are used throughout this paper) in the galaxy MCG-02-38-17 (Arp 261), and spectra identified it as a peculiar Type II SN (P. Garnavich et al. 1995; C. Pollas et al. 1995), showing relative narrow emission components characteristic of SNe IIn (C. Fransson et al. 2002). It was bright at X-ray and radio wavelengths at early times (W. H. G. Lewin et al. 1996; S. D. Van Dyk et al. 1996), making it a member of a small subset of SNe IIn with SNe 1978K, 1986J, 1988Z, and 1998S (C. Fransson et al. 2002). SN 1995N is more radio luminous than many of the observed SNe IIn but less luminous than SN 1988Z (P. Chandra et al. 2009). Its high luminosity and flux evolution imply interaction of the ejecta with inhomogeneous circumstellar matter (CSM; D. W. Fox et al. 2000). The CSM is a gas and dust shell lost by the star before the SN explosion. X-ray observations obtained $\sim$9 yr after the explosion show that the flux dropped by an order of magnitude in 6 yr and could be well fit by thermal emission from CSM interaction, and the higher spatial resolution of the Chandra X-ray Observatory shows that the X-ray light curve of SN 1995N is consistent with a linear decline (P. Chandra et al. 2005; L. Zampieri et al. 2005). SN 1995N was monitored by the VLA for 11 yr beginning soon after the explosion. The radio emission, much like the X-rays, is consistent with bremsstrahlung radiation (P. Chandra et al. 2009).

In this paper, we report new JWST and Keck spectra of SN 1995N obtained over 10,000 days after the SN explosion. SN 1995N is an ideal target for late-time observations, being on the outskirts of its host galaxy and having an extremely slow decline in luminosity (A. Pastorello et al. 2011).

2. Explosion Date

SN 1995N was discovered photometrically on 1995 May 5 and a spectrum was obtained on 1995 May 9 showing that it was "a peculiar Type II supernova" (C. Pollas et al. 1995). They also noted that the spectrum was similar to one obtained of SN 1993N 10 months after its explosion and also to SN 1988Z more than a year after its explosion (M. Turatto et al. 1993). Figure 1 shows a comparison between a spectrum of SN 1995N taken 19 days after discovery with spectra of SN 1993N (age$\sim$9 months) and 1988Z (age$\sim$1 yr). There is also considerable uncertainty about the explosion date for SN 1988Z (R. A. Stathakis & E. M. Sadler 1991). The spectrum of a more recent Type II SN, 2014C, about 1 yr after its explosion, closely resembles the SN 1995N spectrum soon after discovery. It is also plotted in Figure 1 (D. Milisavljevic et al. 2015).

As shown in Figure 1, the SN 1995N spectrum around the time of discovery is most similar to SN 2014C, which is a known SN Ib to IIn transition (D. Milisavljevic et al. 2015). The spectroscopic evolution of SN 2014C is best explained by the explosion of a progenitor star that has been stripped of its hydrogen envelope that is still present as a massive hydrogen-rich shell. The FWHM of the intermediate-width portion of the Hα profile of SN 2014C around 1 yr is around 1200 km s^{-1}. C. Pollas et al. (1995) report a similar velocity width in their discovery spectrum of SN 1995N. This velocity is consistent with the stronger Hα emission and not uncommon among Type IIn SNe where the velocity is interpreted to be the interaction of the ejecta with the H-rich CSM. SN 1995N may have undergone the transition from SN Ib to IIn before it was discovered.

The other spectra shown in Figure 1 are of SN 1993N and 1988Z, the two SNe mentioned as being similar to the SN 1995N discovery spectrum (C. Pollas et al. 1995). SN 1993N was discovered on 1993 April 15 (J. Mueller et al. 1993a). No spectra of SN 1993N have been published previously, but several early-time spectra were obtained with the Kast double spectrograph (J. S. Miller & R. P. S. Stone 1993) on the Lick Shane 3 m telescope; one of them is shown in Figure 1. The Hα emission line for SN 1993N has three components (narrow, intermediate, and broad) indicating CSM interaction and expanding ejecta (A. V. Filippenko & T. Matheson 1993, 1994; J. Mueller et al. 1993b). The spectrum of SN 1993N is more similar to that of SN 1988Z than SN 1995N, which does not show a broad component. Unlike these two SNe, SN 1993N was not detected at radio wavelengths (N. Panagia et al. 2000).

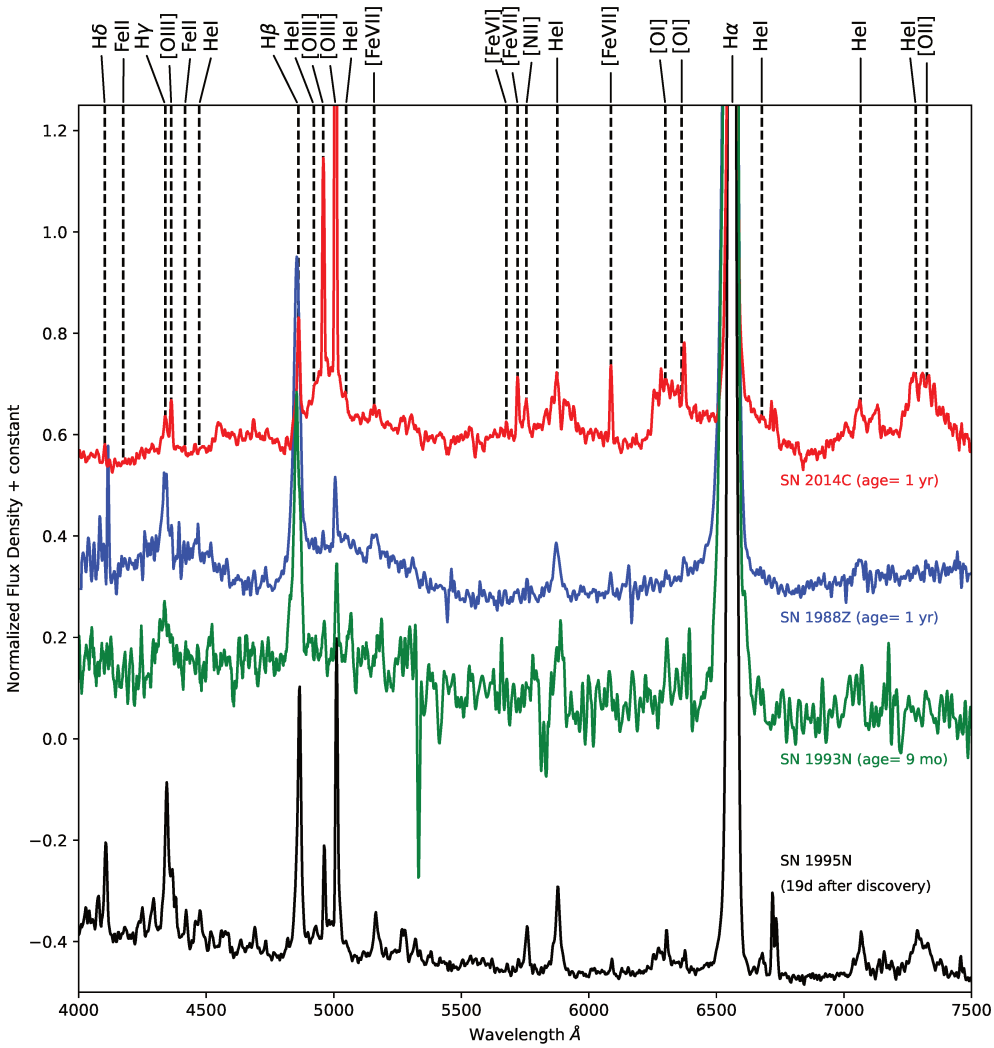

Figure 1. An early-time optical spectrum of SN 1995N taken in 1995 May compared to early-time spectra of SN 2014C, SN 1988Z, and SN 1993N (R. A. Stathakis & E. M. Sadler 1991; M. Turatto et al. 1993; D. Milisavljevic et al. 2015). Flux densities are f_λ.

C. Pollas et al. (1995) also note that coronal lines in the discovery spectrum of SN 1995N resemble those seen in SN 1988Z (M. Turatto et al. 1993). The GELATO[35] SN classification best fit actually picks an even later spectrum of SN 1988Z at day 1149 (A. H. Harutyunyan et al. 2008). The SN 1995N discovery spectrum resembles the 1 yr spectra of SN 1988Z and 2014C, so the assumed age of 10 months at discovery is probably a lower limit (R. A. Stathakis & E. M. Sadler 1991; M. Turatto et al. 1993).

The explosion date has been set to be 1994 July 4 (JD 2449537) assuming that the discovery spectrum, showing a single symmetric Hα emission line, resembled that of SN 1993N about 10 months after the explosion (C. Pollas et al. 1995; C. Fransson et al. 2002). We adopt that date here for easier comparison of the new data presented here with previous papers (e.g., C. Fransson et al. 2002; L. Zampieri et al. 2005; S. D. Van Dyk 2013) although R. Wesson et al. (2023) argue that the width of Hα is not a good discriminator of age, suggesting that the likely age at discovery is actually only $\sim$100 days. No prediscovery observations of SN 1995N have been found.

[35] https://gelato.tng.iac.es/

3. Existing Observations

3.1. Photometry

Almost 27 yr of monitoring of SN 1995N in the *UBVRIJHK* bands is shown in Figure 2 (C. Pollas et al. 1995; B. E. Schaefer & B. Roscherr 1999; B. E. Schaefer 2001; C. L. Gerardy et al. 2002; W. Li et al. 2002; A. Pastorello et al. 2005; L. Zampieri et al. 2005). Photometry from Two Micron All Sky Survey (2MASS), Pan-STARRS, VLT Survey Telescope (VST)-ATLAS, and DENIS is also plotted. The object faded by only about $\Delta V = 1.2$ mag in the first 4 yr after the explosion (W. Li et al. 2002).

SN 1995N already showed a strong near-IR excess when first observed in 1996 July, about 1 yr after the explosion, and observations at $t = 2$–7 yr exhibit a large IR excess consistent with preexisting dust in the CSM (C. L. Gerardy et al. 2002). As shown in Figure 2, the SN was very bright at early times in the *K* band, but mid-IR observations were not obtained of SN 1995N until 2009/2010 serendipitously with the Spitzer Space Telescope and the Wide-field Infrared Survey Explorer (WISE), $\sim$15 yr after the explosion (S. D. Van Dyk 2013). Figure 3 shows the spectral energy distribution (SED) from the *K* band through Spitzer/MIPS 24 μm measured in 2009/2010.

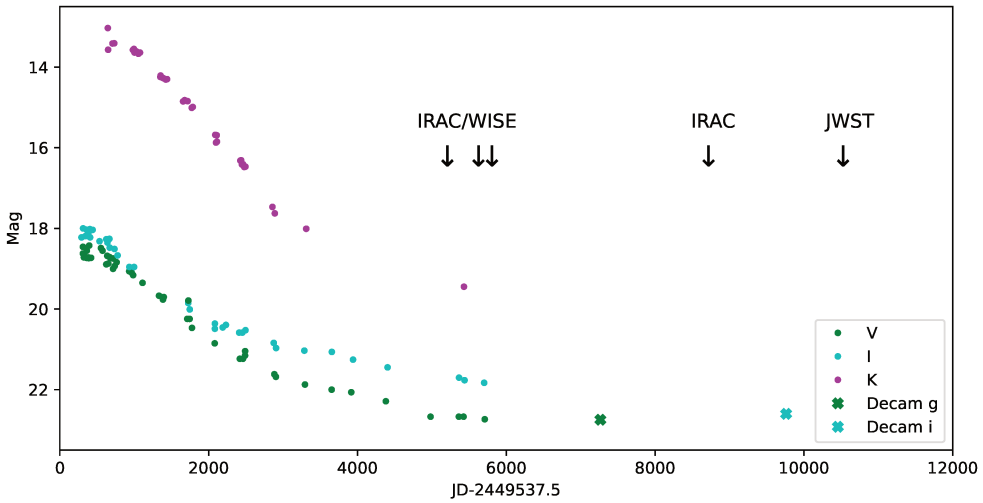

Figure 2. Light curve of SN 1995N covering 26 yr after the explosion (A. Pastorello et al. 2005, 2011). The arrows show the epochs of the IR observations with Spitzer/IRAC, WISE, and JWST.

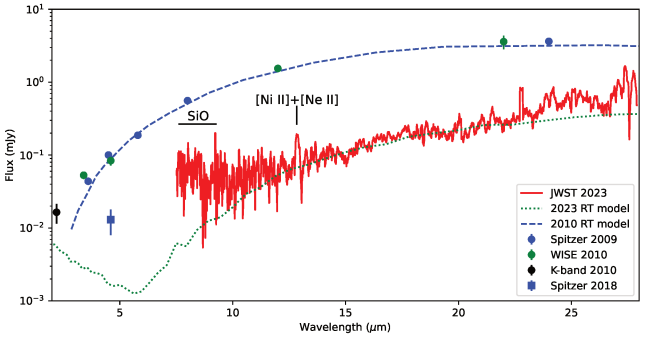

Figure 3. The new JWST/MIRI spectrum is plotted along with the previous IR photometry. The best-fit radiative-transfer models to the 2009–2010 photometry and to the 2023 JWST spectrum are also plotted (R. Wesson et al. 2023).

SN 1995N was also detected by Spitzer/IRAC in the 4.5 μm channel in 2018 (T. Szalai et al. 2021); see Figure 3. The authors note that at an age of $\sim$8600 days, it is the latest observation of an SN IIn in this wavelength band.

The late-time near-IR luminosity can be explained by a simple model where a small fraction of the optical and X-ray radiation is reprocessed into the IR by the interaction between preexisting dusty CSM and the SN shock. As the shock moves away from the region where the bulk of the CSM dust is located, the X-ray and IR dust emission fade away (L. Zampieri et al. 2005).

The NEOWISE and Zwicky Transient Facility archives were searched, but SN 1995N was not detected; however, it was visible in CTIO 4 m/DECam images taken on 2014 May 26 (g, r bands) and 2021 March 25 (i band). Differential photometry was done on these images, showing that SN 1995N was at $g \approx 23.2$ and $r \approx 22.1$ mag in 2014, and $i \approx 23.1$ mag in 2021. These data are plotted in Figure 2.

3.2. Optical Spectra

Three spectra of SN 1995N, obtained on 1995 May 24 (A. V. Filippenko 1997; C. Fransson et al. 2002), 1997 April 11 (C. Fransson et al. 2002), and 2003 July 30 (L. Zampieri et al. 2005) are plotted in Figure 4. Also plotted are two Very Large Telescope (VLT)/XSHOOTER spectra taken in 2010 and 2016 (R. Wesson et al. 2023). Not all of the spectra are flux calibrated, and they are all smoothed using Astropy Box1DKernel to similar spectral resolutions. Other early-time spectra of SN 1995N are shown in C. Fransson et al. (2002), L. Zampieri et al. (2005), and A. Pastorello et al. (2011).

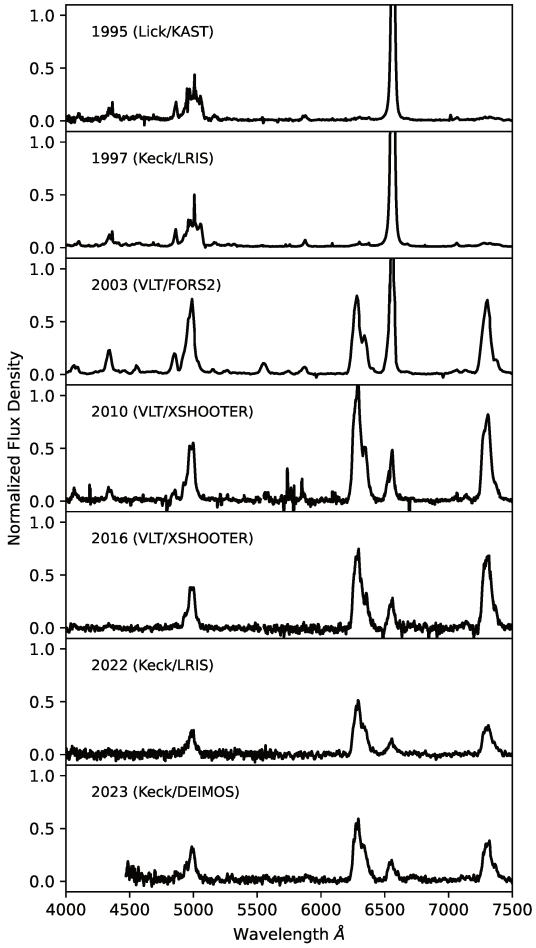

Figure 4. Optical spectra of SN 1995N taken at various epochs from 1995 to 2023. The spectra have been smoothed using Astropy Box1DKernel to similar spectral resolutions. The flux densities (f_λ) have been normalized and shifted. See Sections 3.2 and 4 for details.

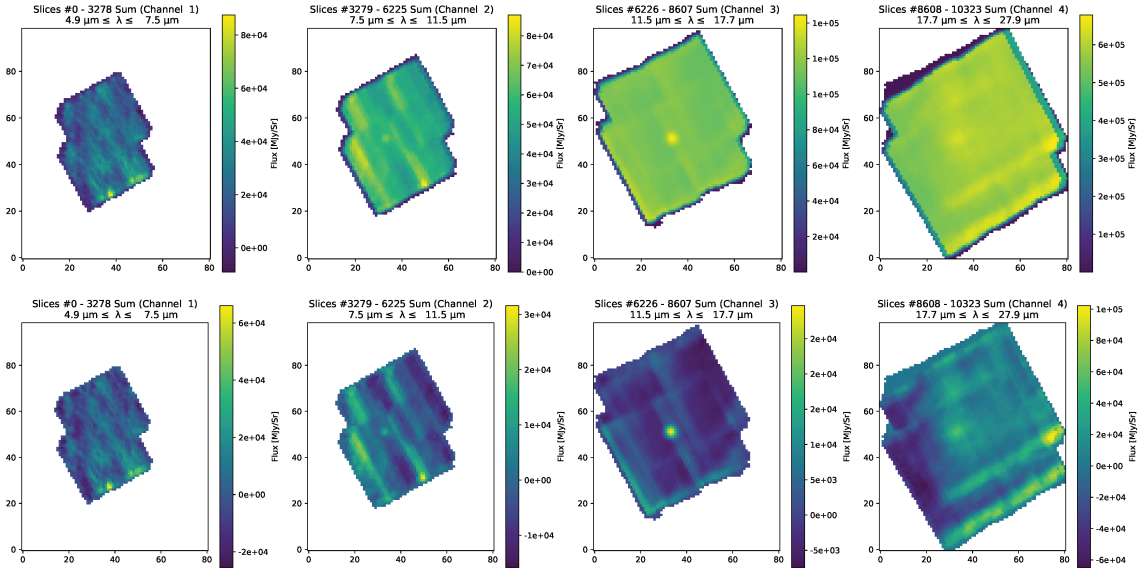

Figure 5. Before (upper) and after (lower) background subtraction stacked images of the data cube in the four channels of MRS for SN 1995N. The emission from SN 1995N can be seen near the centers of all the cubes except in Channel 1.

4. New Observations

New JWST/MRS observations of SN 1995N were obtained on 2023 July 2 (JD 2460129) with the JWST/MIRI MRS, 28 yr (10,286 days) since discovery. The observations include all four channels and all three wavelength ranges of the MRS.

The data consist of $R = \lambda/\Delta\lambda = 1500$–$3500$ spectra spanning 4.9–27.9 μm, including all sub-bands. Dedicated offset background observations were also obtained to provide a more stringent estimate of the local thermal background. These observations are part of GO-1860 (PI: O. Fox). Figure 3 shows the MIRI spectrum of the IR source at the position of SN 1995N as determined by 2MASS.

Level 1 data were initially downloaded from MAST. The data were processed to Level 3 with version 1.11.1 of the JWST calibration pipeline and context jwst-1183 of the Calibration Reference Data System. The standard MRS pipeline procedure was followed (H. Bushouse et al. 2024). This step automatically includes the dedicated background observations for subtraction. Figure 5 shows the collapsed cube in each channel both before and after the dedicated background subtraction.

We note that the global thermal background is roughly 5 orders of magnitude larger than the SN 1995N flux; thus, estimating the local background is challenging. Even small variability in the background across the field of view can have a potentially large impact on the source spectrum, especially at the longest wavelengths where the background tends to be the largest and the signal-to-noise ratio (S/N) of the source tends to be the smallest.[36]

Furthermore, while the dedicated background removes the majority of the global thermal background, it does not take into account the local background of SN 1995N (see Figure 5). The background-subtraction method is described in detail by M. Shahbandeh et al. (2025).

[36] https://www.stsci.edu/contents/news/jwst/2023/miri-mrs-reduced-count-rate-update

Spectra of the SN were extracted using the JWST pipeline `extract_1d` step. For point sources, the pipeline uses a circular extraction aperture, which varies in radius with wavelength. The extraction-related vectors are found in the Advanced Scientific Data Format `extract1d` reference file. We use the default reference file and aperture correction. Figure 3 shows the final MRS extraction of SN 1995N. Analysis of the data cubes shows that flux from the position of SN 1995N is visible starting around 7.6 μm, so the spectrum has been truncated below that wavelength.

Unpublished optical spectra of SN 1995N taken with Lick/KAST on 1995 May 24 and 1997 April 11 are shown in Figure 4. New optical spectra were obtained with the Keck 10 m telescopes on Maunakea using LRIS (J. B. Oke et al. 1995) on 2022 March 04 and DEIMOS (S. M. Faber et al. 2003) on 2023 April 23. The LRIS observation used the 1″ slit, 600/4000 grism, and 400/8500 grating. Data reduction followed standard techniques using the LPipe data-reduction pipeline (J. M. Silverman et al. 2012; D. A. Perley 2019). These spectra are plotted in Figure 4.

5. Spectral Evolution

Optical and ultraviolet spectra of SN 1995N, obtained 1–5 yr after the explosion, indicate the presence of two velocity components with narrow (500 km s^{-1}) and intermediate (1700 km s^{-1}) line widths (C. Fransson et al. 2002). They also suggest that the Hα emission profile has faint broad wings, but looking at their Figure 3 and the spectra presented here, including one taken soon after discovery, there is no indication of broad wings in Hα other than possibly the 1997 April 11 epoch. This spectrum was obtained about 3 yr after explosion. The intermediate-width component dominates. Moreover, Hβ does not have a broad profile. Nonetheless, even if some of this broad extension is attributable to Hα, it could indicate that the star was not completely stripped at the time of explosion. SN 2014C had high-velocity H absorption in the photospheric-epoch spectra, meaning the star was not completely stripped; no strong evidence for H emission at late

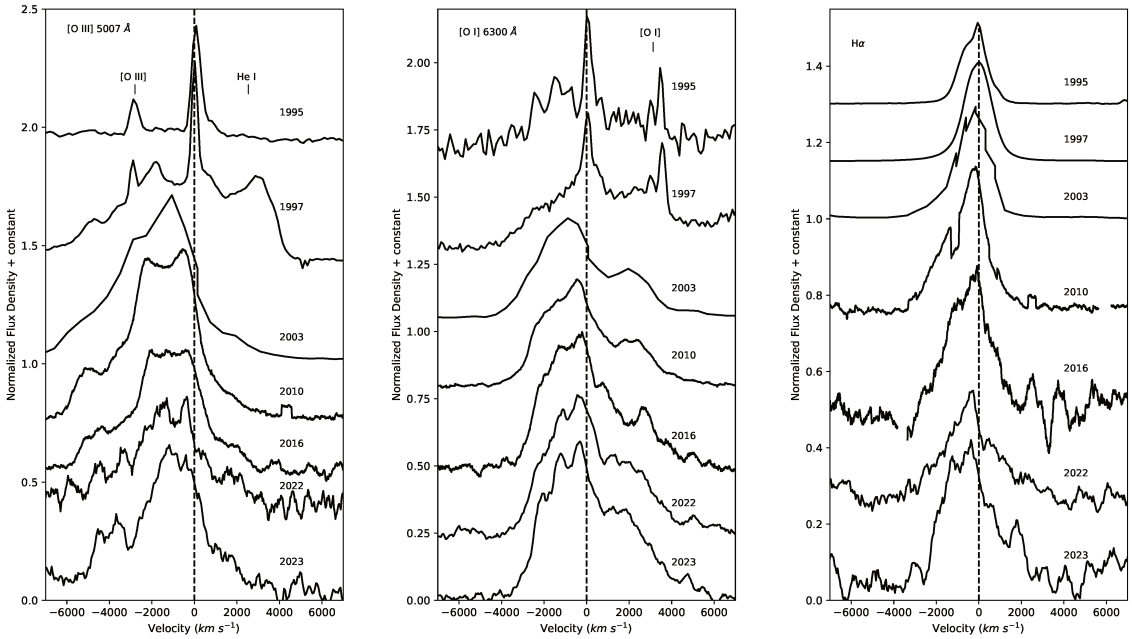

Figure 6. Optical spectra of SN 1995N taken at various epochs from 1995 to 2023 in velocity space for [O III] 5007 Å, [O I] 6300 Å, and Hα 6563 Å. The spectra were smoothed using Astropy Box1DKernel to similar spectral resolutions. The flux densities (f_λ) have been normalized and shifted. See Sections 3.2 and 4 for details. The rest wavelengths of [O III] 4959 Å, He I 5048 Å, and [O I] 6364 Å are marked.

epochs associated with ejecta was observed. SN 1995N could be a case where more hydrogen was present in the envelope at the time of core collapse. It is important to note that the broad Hα was not observed at the time of discovery (See Figure 1), which indicates that hydrogen was not predominant in the envelope of the progenitor star at the time of explosion.

Figures 4 and 6 show the evolution of the optical spectra of SN 1995N over 28 yr. The most obvious change with time is seen in Hα, whose line profile was quite symmetric at early times but has evolved with the red wing fading faster than the blue wing, an indication of dust formation in the ejecta. The asymmetry in Hα first becomes visible in a spectrum taken in 1999, 1799 days past explosion (C. Fransson et al. 2002; R. Wesson et al. 2023). The asymmetry in the hydrogen emission lines is also noted in a VLT spectrum taken on 2003 July 30 (L. Zampieri et al. 2005).

In the VLT XSHOOTER spectra from 2010 and 2016, as well as the new Keck spectra from 2022/2023, the continued evolution can be seen in Figures 4 and 6. When these spectra were obtained, SN 1995N was faint, $V \approx 23$ mag. The optical brightness did not change much from 2010 to 2021, as shown in Figure 2. Strong, broad emission from [O I] $\lambda\lambda$6300, 6364, [O II] $\lambda\lambda$7319, 7331, and [O III] $\lambda\lambda$4959, 5007are seen in the spectra taken from 2010 to 2023. Hα is weaker but also clearly detected. Between 2003 and 2010, the [O I], [O II], and [O III] lines became much stronger relative to Hα. By 2010, the oxygen lines are far stronger than Hα, and this great strength has remained through 2023. In Figure 1 of A. Pastorello et al. (2011), which shows the evolution of the optical spectrum of SN 1995N between 1995 and 2010, the strengthening of the [O I] and [O II] emission begins as early as 1998, and by 2004, these lines are nearly as strong as Hα. As seen in Figure 3 of S. Tinyanont et al. (2025), SN 2014C is undergoing a very similar spectral evolution to SN 1995N. Between 7 and 8.5 yr after explosion, the oxygen emission lines in SN 2014C strongly increase compared to Hα.

6. The JWST Spectrum

The JWST/MRS spectrum is plotted in Figure 3 along with Spitzer and WISE photometry to show how the IR emission has evolved over time. The emission feature seen at $\sim$13 μm is probably a blend of [Ni II] 12.729 μm and [Ne II] 12.813 μm, seen strongly in the IR spectrum of SN 2004dj on day 868 (R. Kotak et al. 2006; T. Szalai et al. 2011). The [Ne II] emission line is one of the primary coolants for the ejecta (R. A. Chevalier & C. Fransson 1992). SN 2014C also shows a strong [Ne II] emission line in its MIRI spectrum almost 10 yr after its explosion (S. Tinyanont et al. 2025). The S/N is low, but the plateau-like feature between 7.6 and 9 μm may be molecular emission due to the SiO fundamental band as previously seen in SNe 1987A, 2003gd, 2004et, and 2005af (D. H. Wooden et al. 1993; R. Kotak et al. 2006; W. P. S. Meikle et al. 2007; A. Jerkstrand et al. 2012). D. H. Wooden et al. (1993) found that the SiO feature disappeared in SN 1987A when dust formation occurred after day 400. This detection in SN 1995N, if real, would be at a much later time than previous detections in other SNe.

7. Radiative-transfer Modeling

The dust associated with SN 1995N consists of dust in the circumstellar shell that may have existed before the explosion and newly formed dust that may lie in the unshocked ejecta not yet hit by the reverse shock or in the cool dense shell between the forward and reverse shocks (R. Wesson et al. 2023).

Before 2009, there were no IR observations of SN 1995N to the red of the K band. The large excess in the K-band photometry undoubtedly results from emission by warm dust but cannot be used to estimate dust masses (C. L. Gerardy et al. 2002).

S. D. Van Dyk (2013) modeled the 2009/2010 dust emission detected using Spitzer/IRAC at 3.6, 4.5, 5.8, and 8.0 μm and Spitzer/MIPS at 24 μm, as well as with WISE at 3.4, 4.6, 12,

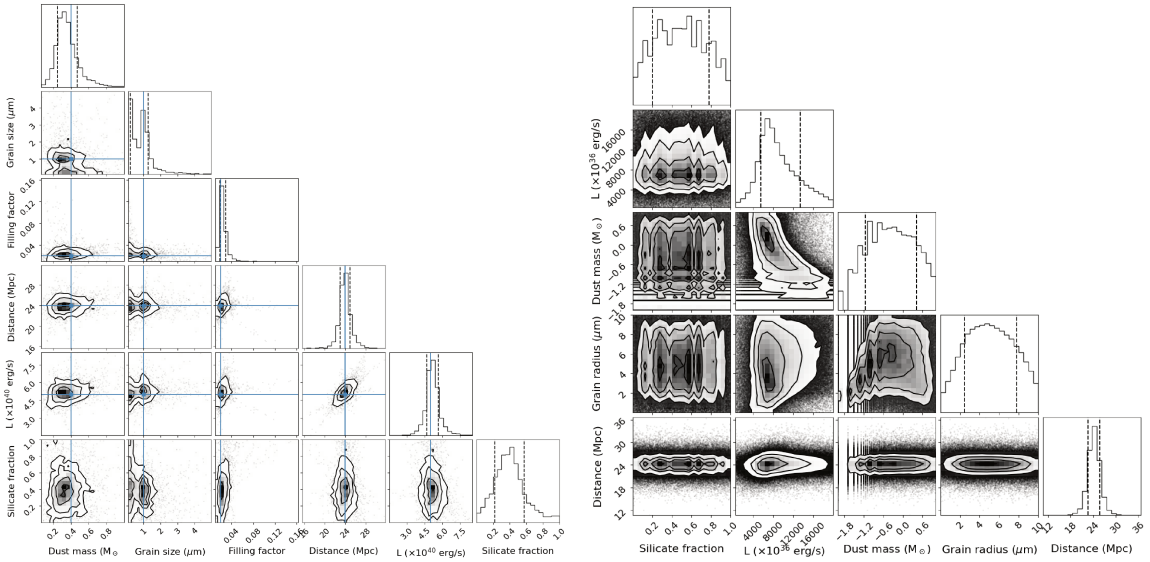

Figure 7. The results of the MCMC analysis of the MOCASSIN models for the Spitzer/WISE 2009–2010 epoch on the left and for the JWST 2023 epoch on the right. The parameters are silicate fraction, heating source luminosity, dust mass, grain size, and distance. Vertical dashed lines indicate 1σ confidence intervals. Blue crosshairs in the left panel indicate the values found by R. Wesson et al. (2023) from an analysis of a much smaller grid of models than used here.

Table 1
Best MOCASSIN Models

Model	χ^2	Sil. Frac.	L (10^{39} erg s^{-1})	M_d ($M_\odot$)	Grain Size (μm)	Distance (Mpc)
Spitzer/WISE Models	⋯	0.405 ± 0.192	51.8 ± 6.3	0.36 ± 0.13	0.9 ± 0.7	24.0 ± 1.3
JWST models:						
$M_d = 0.4\,M_\odot$	9230.6	0.05	9.0	0.40	3.8	27.5
Best of all fits	4031.2	0.43	6.1	2.62	6.2	25.1
>90% silicates	4776.2	0.94	6.0	3.64	8.1	24.3
>90% carbon	4896.2	0.01	6.7	0.82	4.4	24.0
$M_d < 1.0\,M_\odot$	5371.5	0.11	7.3	0.87	4.1	26.6
Grain size< 1 μm	9194.6	0.77	5.4	0.04	0.9	23.4

and 22 μm. They used an "idealized dust cloud," which is just an optically thin point source, to model the dust emission from the Spitzer/WISE photometry. These models were calculated using astronomical silicate and graphite grains with a size of 0.1 μm. The model results imply a dust mass of 0.05 $M_\odot$ for silicate grains and 0.12 $M_\odot$ for graphite grains. S. D. Van Dyk (2013) suggest that the dust is cool, ∼240 K, and likely is preexisting dust from circumstellar mass loss before the explosion.

R. Wesson et al. (2023) remodeled the Spitzer and WISE data used by S. D. Van Dyk (2013). They employed the three-dimensional radiative-transfer code MOCASSIN (B. Ercolano et al. 2005) and found a best-fit model with 0.4 $M_\odot$ of 1 μm amorphous carbon dust grains, in a clumpy shell with a volume filling factor of 0.02. We have revisited these models, expanding the parameter space investigated to include silicate dust and using the Markov Chain Monte Carlo (MCMC) ensemble sampler `emcee` (D. Foreman-Mackey et al. 2013) to improve the sampling of the parameter space investigated by R. Wesson et al. (2023).

We construct the models similarly to those presented in R. Wesson et al. (2023); our new models assume that the velocity of the outermost ejecta is 5000 km s^{-1}, and the inner radius of the ejecta was set to 0.2× the outer radius. The clumpy dusty ejecta is heated by a diffuse source located in the interclump medium, with a temperature of 5000 K. We ran models with free parameters and their adopted priors as listed below. All priors are uniform unless stated.

1. Dust mass: 10^{-3}–1.0 $M_\odot$
2. Grain size: 0.1–5 μm
3. Clump volume filling factor: 0.01–0.5
4. Source luminosity: $10^{40\text{–}41}$ erg s^{-1}
5. Silicate fraction: 0–1
6. Distance: Gaussian prior with a mean of 24.1 Mpc and standard deviation of 1.6 Mpc (taken from the NASA Extragalactic Database, and consistent with that adopted by previous studies; C. Fransson et al. 2002; S. D. Van Dyk 2013)

Figure 7 shows the MCMC corner plot for these models, with the values found by R. Wesson et al. (2023) indicated with blue crosshairs. Our remodeling is in excellent agreement with the values from R. Wesson et al. (2023) for all parameters except for the silicate fraction, which was constrained to zero by R. Wesson et al. (2023). In our reanalysis, we find that low but nonzero values are preferred with a best-fitting value of 0.41 ± 0.19. The best-fitting parameters are listed in Table 1, and the corresponding fit is plotted in Figure 3.

Optical spectra presented by C. Fransson et al. (2002) and VLT/XSHOOTER spectra obtained in 2010 and 2016 were also modeled using DAMOCLES (A. Bevan & M. J. Barlow 2016), a code that calculates the profiles of emission lines arising within the expanding ejecta including the effects of dust embedded in the ejecta (R. Wesson et al. 2023). The spectra that were fit are plotted in Figure 4. The C. Fransson et al. (2002) spectrum from 1999 (JD 2451126) was modeled, and a dust mass of $2 \times 10^{-4}\,M_{\odot}$ was found. The best-fit dust masses for the 2010 and 2016 spectra estimated with this alternative emission-line method were consistent with the MOCASSIN results of $0.4\,M_{\odot}$ for the 2009/2010 IR epoch but are also well fit with dust masses greater than $0.1\,M_{\odot}$.

New MOCASSIN models were constructed to fit the JWST data presented here. As a starting point, we took the best-fit model grid and clump parameters from R. Wesson et al. (2023) and then expanded the grid to the epoch of the JWST spectra to take into account the expansion of the ejecta between 2010 and 2023. That best-fit model has $0.4\,M_{\odot}$ of amorphous carbon dust in the form of 1 μm grains, distributed in a clumpy shell with a volume filling factor of 0.02. The grid that fit the observations in 2009–2010 was enlarged by assuming constant homologous expansion. Models with all parameters unchanged except the grid size significantly overpredict the JWST fluxes. The heating source has therefore significantly declined in luminosity since 2009–2010.

Therefore, models were constructed with an expanded grid and a reduced source luminosity. These can broadly fit the JWST observations. Thus, a scenario in which dust formation was complete by 2009–2010, and the dust existing at that epoch has since expanded and cooled, may be able to account for the observed SED in 2023.

To assess the range of parameters that can fit the JWST data, we explored a much larger range of parameters using the MCMC ensemble sampler `emcee` (D. Foreman-Mackey et al. 2013). Approximately 320,000 models were run to sample the parameter space that we describe briefly here.

1. Distance: we take a Gaussian prior with a mean of 24.1 Mpc and standard deviation of 1.6 Mpc (taken from the NASA Extragalactic Database and consistent with that adopted by previous studies; C. Fransson et al. 2002; S. D. Van Dyk 2013).
2. Heating source luminosity: the dust in the models is heated by a diffuse source distributed uniformly in the interclump regions of the expanding dust shell. Physically, this is consistent with a scenario in which the energy source powering the dust emission is the interaction between the ejecta and CSM, but rather than directly heating the dust, this interaction heats gas within the ejecta, which in turn heats the dust. The luminosity of the heating source will depend on the extent of the ejecta–CSM interaction and has clearly declined significantly since the 2009–2010 Spitzer/WISE data. We adopt a uniform prior with value of (5–200) $\times\ 10^{38}$ erg s^{-1}.
3. Grain size: our models assume a single grain size. A distribution of grain sizes is more realistic but would require at least two more free parameters (upper and lower limits and power-law exponent for an MRN-type grain-size distribution; J. S. Mathis et al. 1977) on which few observational constraints are available. We therefore use only a single grain size, with an assumed uniform prior from 0.005 to 10 μm.
4. Silicate fraction: R. Wesson et al. (2023) argue that silicate dust was unlikely to be present within the ejecta in 2009–2010, owing to the absence of large red scattering wings in optical emission lines. Nevertheless, we consider the possibility that some silicate dust has subsequently formed and assume a uniform prior from zero to unity of the silicate fraction.
5. Dust mass: we adopt a broad and uniform prior in log space for the dust mass, extending from 10^{-2} to $10^{1}\,M_{\odot}$.

The JWST spectrum was resampled to match the sampling of the MOCASSIN output SED, and the likelihood function was taken as the sum of the χ^2 values obtained by comparing model fluxes to the observations. Two-hundred walkers were used for 2500 iterations to explore the parameter space and estimate the posterior probability distributions.

The results of the MCMC analysis of the parameter space are shown in Figure 7. The heating source luminosity is well constrained at $\sim 8 \times 10^{39}$ erg s$^{-1} = 2 \times 10^{6}\,L_{\odot}$, given the assumptions for the distance. The silicate fraction is not well constrained by the data. At very late times, the dust in SN ejecta can be cold enough, or the grains large enough, that the SED of silicate dust is quite featureless (T. Henning 2010). Dust masses below $0.1\,M_{\odot}$ are strongly disfavored, and dust grains several microns in radius are preferred. Dust masses of $\sim 1\,M_{\odot}$ give the best fits, but they are not well constrained either. Lower dust masses require higher luminosities and smaller grains.

The best fits for various parameter values are shown in Figure 8, and the parameters of these models are given in Table 1. Figure 8 demonstrates how similar many of the fits are, and although the χ^2 values listed in Table 1 differ, the fits appear very similar to the eye. To calculate χ^2 values, we resample the observations to the lower spectral resolution provided by our radiative-transfer simulations, and this resampling gives reduced noise in each spectral element, such that the minor differences between observations and predicted SEDs that give rise to the differences in χ^2 values are not clearly visible on the log-scale figures.

As can be seen from the examples in Table 1, many of the best fits have dust masses significantly greater than the $0.4\,M_{\odot}$ inferred from the modeling of the 2009/2010 photometry. This suggests that dust formation in SN 1995N could be continuing between 2009–2010 and 2023, although some of the inferred dust masses are unprecedented. R. Wesson et al. (2023) found that a grain size of 1 μm gave the best fit to the 2009–2010 SED, while the current analysis suggests larger grains still, pointing to possible accretion onto previously formed grains as a likely mechanism for the continuing dust-mass growth.

8. The Evolution of SN 1995N

C. Fransson et al. (2002) found that the velocities and densities measured from the narrow lines in the early-time spectra of SN 1995N were typical for the CSM of red supergiants. They also suggested that the SN 1995N progenitor was similar to the highly luminous red supergiant VY CMa and the post-red-supergiant IRC +10420, which have superwinds and initial masses of at least $30\,M_{\odot}$. This kind of extreme mass-loss rate is required to account for the dense CSM and strong SN–CSM interaction seen in SN 1995N. The

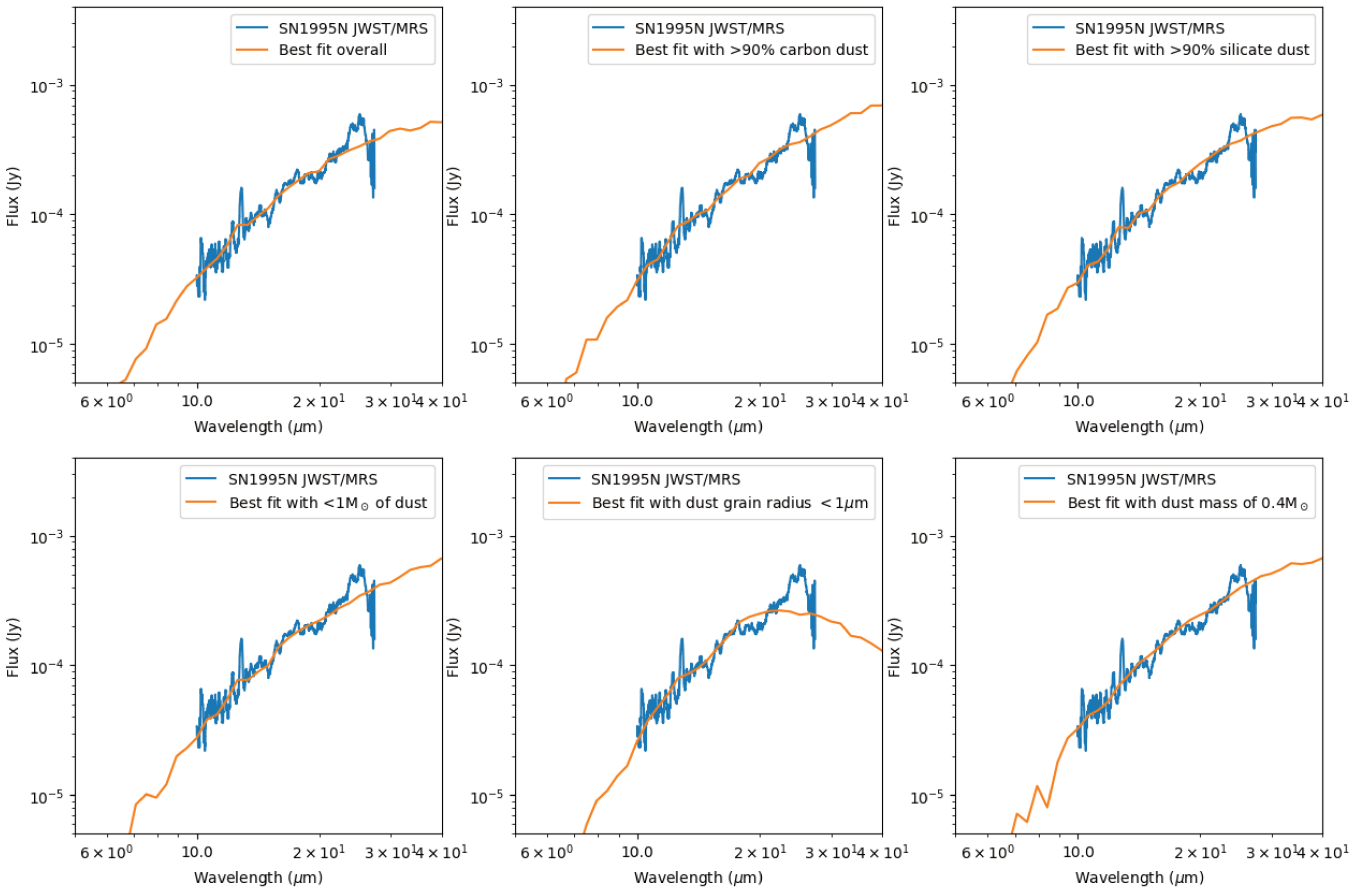

Figure 8. Best-fit MOCASSIN models for the new JWST spectrum; see Table 1.

dust-emitting volume of SN 1995N, $r \approx 10^4$ au, is compatible with the size of the CSM around VY CMa and IRC +10420, and the estimated mass of the SN 1995N progenitor nebula agrees with those found for the two Galactic stars (S. D. Van Dyk 2013).

The emission from SN 1995N comes from clumps in the X-ray-photoionized, preshock, circumstellar gas (narrow lines) and also shocked gas interacting with clumpy or asymmetric CSM (intermediate lines) (C. Fransson et al. 2002; M. Shahbandeh et al. 2025). It is likely that all the emission components are heated and ionized by high-energy radiation from the interaction region. These mechanisms were also suggested to explain the observations of SN 1988Z (N. N. Chugai & I. J. Danziger 1994).

The later-time evolution of the SN 1995N spectrum can be seen in Figures 4 and 6. The most obvious change with time is in Hα, whose line profile was quite symmetric at early times but starting in 1999, about 5 yr after the explosion, evolved with the red wing fading faster than the blue wing, an indication of dust formation in the ejecta (C. Fransson et al. 2002; R. Wesson et al. 2023).

To get to the observer, redshifted photons from the receding far edge of the ejecta must pass through the dust mixed with the expanding ejecta, while the blueshifted photons from the approaching near edge do not, resulting in more attenuation of the red wing of intrinsically symmetric emission lines. There is also dust in the preexisting CSM, but the higher velocities shown here indicate dust has formed in the ejecta. This is clearly visible in Figure 6, which shows how the [O III], [O I], and Hα emission lines evolve in velocity space. Also, a blue/red asymmetry clearly developed after 1–2 yr in the intermediate-width Hα component, suggesting that some of the new dust is in the cool dense shell behind the shock.

The SN–CSM interaction began sometime before the discovery spectrum was obtained $\geqslant$10 months after the explosion. SN 1995N was very bright at X-ray and radio wavelengths, indicating a strong ejecta–CSM interaction. The X-rays produced by the interaction with photoionized hydrogen in the CSM shell lead to Hα emission. The SN–CSM interaction also caused a reverse shock to form that moved back into the expanding ejecta (D. Milisavljevic & R. A. Fesen 2017). Eventually, this reverse shock reached the inner ejecta region, ionizing the metal-rich gas from which the optical lines are produced. This caused the [O I], [O II], and [O III] emission lines to strengthen until they became stronger than Hα. This is part of the transition from SN to SNR, when the radioactive ^{56}Co heating of the O-rich inner ejecta gives way to the reverse-shock excitation (D. Milisavljevic & R. A. Fesen 2017). Such an abrupt change in emission is rarely observed in SNe, but it is an important step in the transition from SN to SNR. It also implies that the SN 1995N progenitor was fully or partially stripped of its H-rich envelope before the explosion.

A similar metamorphosis where the O emission becomes stronger than the H emission is seen in late-time spectra of SN 1996cr (D. Patnaude et al. 2025). Like SN 1995N, SN 1996cr was also discovered long after its explosion after first being detected as an X-ray source. Two other SNe, SN 2001em and SN 2014C, exploded as stripped-envelope SNe but later

interacted with H-rich circumstellar shells, changing them from Type Ib/c to IIn (N. N. Chugai & R. A. Chevalier 2006; D. Milisavljevic et al. 2015). The spectroscopic evolution of SN 2014C is very similar to that seen on SN 1995N on the same timescales (S. Tinyanont et al. 2025). Neither SN 1995N nor SN 1996cr has spectra taken near the time of the explosion, so the early Type Ib/c phase may have been missed. Both SN 1996cr and SN 1995N underwent a major episode of mass loss before their explosions.

The dust associated with SN 1995N includes preexisting dust in the CSM, which is heated by the initial flash and then by the ejecta–CSM interaction. The dust emission is seen in *K*-band emission early, but no estimate of the dust mass can be made because Spitzer/WISE photometry is not available until 2009/2010, 14 yr after the explosion. The dust formation in the ejecta began in the late 1990s. Dust can also form in the cool dense shell behind the forward shock. The dust measured in the 2009/2010, 2018, and 2023 IR observations could be in the CSM, ejecta, or cool dense shell; these alternatives cannot be distinguished.

The DAMOCLES code (A. Bevan & M. J. Barlow 2016), which fits [O I], [O III], and Hα emission-line profiles in the optical, estimates only the mass of dust in the ejecta (R. Wesson et al. 2023). DAMOCLES was used to fit optical spectra of SN 1995N obtained between 1996 and 2016 (C. Fransson et al. 2002; R. Wesson et al. 2023). Assuming amorphous carbon dust, the dust mass in the ejecta from 1996 to 1999 is $\lesssim 10^{-4}\,M_{\odot}$. For spectra obtained in 2010 and 2016, the dust mass is $\gtrsim 0.1\,M_{\odot}$. In particular, the 2010 DAMOCLES estimate and the 2009/2010 MOCASSIN estimate are both compatible with a dust mass of $\sim 0.4\,M_{\odot}$. So, most or all of the dust mass in that epoch could be embedded in the ejecta and formed sometime after 1999, about 4 yr after the explosion. There is no IR photometry until $\sim$15 yr after the explosion, so a comparison with the emission-line dust-mass estimates is not possible at early times.

The dust mass in 2009/2010 estimated through MOCASSIN radiative-transfer modeling is $0.36 \pm 0.13\,M_{\odot}$ (R. Wesson et al. 2023). The estimated dust mass in 2023 using the JWST spectrum is $0.42^{+2.16}_{-0.35}\,M_{\odot}$. SN 2014C also has dust in much smaller amounts than estimated for SN 1995N. But SN 2014C is only 10 yr old (S. Tinyanont et al. 2025).

9. Conclusions

The early-time spectra of SN 1995N exhibit narrow and intermediate emission lines, arising respectively from the photoionized CSM shell and the interaction of the CSM lost by the star before the explosion with the ejecta. The narrow lines imply a dense, massive CSM shell resulting from a large red-supergiant mass-loss episode shortly before the SN explosion. This mass loss partially or fully stripped the envelope, so SN 1995N could have been intrinsically a Type Ib/c SN shortly after the explosion, but the CSM interaction began before the discovery spectrum was obtained nearly a year later. The result is a very unusual late-time spectrum where the oxygen-forbidden emission lines are much stronger than Hα. This occurs when the reverse shock begins to interact with and excite the O-rich, H-poor inner ejecta. The spectral evolution indicates that the transition from SN to SNR has begun (e.g., D. Milisavljevic & R. A. Fesen 2008). The strong similarities between SN 1995N and 2014C, which is known to be a stripped SN that transitioned from Ib to IIn, supports the idea that SN 1995N has had the same evolution (D. Milisavljevic et al. 2015; S. Tinyanont et al. 2025). But, because there are no early-time observations of SN 1995N, there cannot be certainty.

The dust associated with SN 1995N includes preexisting dust in the CSM, as well as later-forming dust in the expanding ejecta or the cool dense shell behind the forward shock. The IR observations measure the total dust mass in these three locations, while the emission-line fitting measures only the dust forming in the ejecta.

As shown in Figure 7, the dust shell inferred by R. Wesson et al. (2023) can account for the JWST spectrum without difficulty if it has uniformly expanded in the meantime and the heating source has faded. While a fit is possible with many different combinations of parameters, the whole ensemble suggests that both the dust mass and grain size have increased between 2010 and 2023.

However, these are the best models that can be produced considering that the data only cover $\sim$7–27 μm. The estimate of the dust mass is not well constrained in the absence of data longward of 27 μm. When one looks at Figure 8, the differences among the fits are quite small. The model with the same dust mass as in 2010, $0.4\,M_{\odot}$, along with the expansion of the ejecta and fading of the heating source over the last decade, is perhaps the most likely using Occam's razor. A dust mass of $0.4\,M_{\odot}$ is also more consistent with the masses observed in other older CCSNe. A large mass of cold dust such as that seen in SN 1987A would not be detected in these observations (M. Matsuura et al. 2011, 2015).

As shown in Figure 16 of R. Wesson et al. (2023), SN 1995N is one of the oldest Type II SNe where IR dust emission and optical emission lines can still be detected, over 10,000 days postdiscovery. More observations of CCSN dust emission at extremely late times are needed that extend further into the IR. Until then, it will be difficult to choose between the two dust-formation scenarios—continuous dust formation or most (or all) of the dust forms at early times following the SN explosion (E. Dwek & R. G. Arendt 2015; A. Bevan & M. J. Barlow 2016; E. Dwek et al. 2019; R. Wesson et al. 2023).

Similarly, the very late-time optical spectra allow a rare view into the inner ejecta excited by the reverse shock, showing the transition from SN to SNR.

Acknowledgments

We thank the anonymous referee for suggestions that have improved the paper. This work is based (in part) on observations made with the NASA/ESA/CSA James Webb Space Telescope. The data were obtained from the Mikulski Archive for Space Telescopes at the Space Telescope Science Institute, which is operated by the Association of Universities for Research in Astronomy, Inc., under NASA contract NAS 5-03127 for JWST. The observations are associated with program GO-1860.

The specific observations analyzed can be accessed via doi:10.17909/04jm-tx25. Support to MAST for these data is provided by the NASA Office of Space Science via grant NAG5-7584 and by other grants and contracts.

Partial support for this work was provided by NASA grant JWST-GO-02666.002-A. S.Z. received support from the NKFIH OTKA K142534 grant. A.V.F.'s research group at UC Berkeley acknowledges financial assistance from the

Christopher R. Redlich Fund, as well as donations from Gary and Cynthia Bengier, Clark and Sharon Winslow, Alan Eustace and Kathy Kwan, William Draper, Timothy and Melissa Draper, Briggs and Kathleen Wood, and Sanford Robertson (W.Z. is a Bengier-Winslow-Eustace Specialist in Astronomy, T.G.B. is a Draper-Wood-Robertson Specialist in Astronomy, Y.Y. was a Bengier-Winslow-Robertson Fellow in Astronomy), and many other donors. D.M. acknowledges support from the National Science Foundation (NSF) through grants PHY-2209451 and AST-2206532.

The W. M. Keck Observatory is operated as a scientific partnership among the California Institute of Technology, the University of California, and NASA; the observatory was made possible by the generous financial support of the W. M. Keck Foundation. The Kast spectrograph on the Shane 3 m telescope at Lick Observatory was made possible through a generous gift from William and Marina Kast. We acknowledge the excellent assistance of the staff at each of Keck and Lick Observatories.

ORCID iDs

Geoffrey C. Clayton https://orcid.org/0000-0002-0141-7436
R. Wesson https://orcid.org/0000-0002-4000-4394
Ori D. Fox https://orcid.org/0000-0003-2238-1572
Melissa Shahbandeh https://orcid.org/0000-0002-9301-5302
Alexei V. Filippenko https://orcid.org/0000-0003-3460-0103
Bryony Nickson https://orcid.org/0000-0002-9915-1372
Michael Engesser https://orcid.org/0000-0003-0209-674X
Schuyler D. Van Dyk https://orcid.org/0000-0001-9038-9950
WeiKang Zheng https://orcid.org/0000-0002-2636-6508
Thomas G. Brink https://orcid.org/0000-0001-5955-2502
Yi Yang https://orcid.org/0000-0002-6535-8500
Tea Temim https://orcid.org/0000-0001-7380-3144
Nathan Smith https://orcid.org/0000-0001-5510-2424
Jennifer Andrews https://orcid.org/0000-0003-0123-0062
Chris Ashall https://orcid.org/0000-0002-5221-7557
Ilse De Looze https://orcid.org/0000-0001-9419-6355
James M. Derkacy https://orcid.org/0000-0002-7566-6080
Luc Dessart https://orcid.org/0000-0003-0599-8407
Eli Dwek https://orcid.org/0000-0001-8033-1181
Ryan J. Foley https://orcid.org/0000-0002-2445-5275
Suvi Gezari https://orcid.org/0000-0003-3703-5154
Sebastian Gomez https://orcid.org/0000-0001-6395-6702
Jacob Jencson https://orcid.org/0000-0001-5754-4007
Joel Johansson https://orcid.org/0000-0001-5975-290X
Mansi Kasliwal https://orcid.org/0000-0002-5619-4938
Zachary G. Lane https://orcid.org/0009-0003-8380-4003
David Law https://orcid.org/0000-0002-9402-186X
Anthony Marston https://orcid.org/0000-0001-5788-5258
Dan Milisavljevic https://orcid.org/0000-0002-0763-3885
Richard O'Steen https://orcid.org/0000-0002-2432-8946
Justin Pierel https://orcid.org/0000-0002-2361-7201
Armin Rest https://orcid.org/0000-0002-4410-5387
Arkaprabha Sarangi https://orcid.org/0000-0002-9820-679X
Matthew Siebert https://orcid.org/0000-0003-2445-3891
Lou Strolger https://orcid.org/0000-0002-7756-4440
Tamás Szalai https://orcid.org/0000-0003-4610-1117
Samaporn Tinyanont https://orcid.org/0000-0002-1481-4676
Qinan Wang https://orcid.org/0000-0001-5233-6989
Brian Williams https://orcid.org/0000-0003-2063-381X
Lin Xiao https://orcid.org/0000-0002-6986-5593
Szanna Zsíros https://orcid.org/0000-0001-7473-4208

References

Barlow, M. J., Krause, O., Swinyard, B. M., et al. 2010, A&A, 518, L138
Bertoldi, F., Carilli, C. L., Cox, P., et al. 2003, A&A, 406, L55
Bevan, A., & Barlow, M. J. 2016, MNRAS, 456, 1269
Bushouse, H., Eisenhamer, J., Dencheva, N., et al. 2024, JWST Calibration Pipeline, v1.19.1, Zenodo, doi:10.5281/zenodo.6984365
Chandra, P., Ray, A., Schlegel, E. M., Sutaria, F. K., & Pietsch, W. 2005, ApJ, 629, 933
Chandra, P., Stockdale, C. J., Chevalier, R. A., et al. 2009, ApJ, 690, 1839
Chevalier, R. A., & Fransson, C. 1992, ApJ, 395, 540
Choban, C. R., Salim, S., Kereš, D., Hayward, C. C., & Sandstrom, K. M. 2025, MNRAS, 537, 1518
Chugai, N. N., & Chevalier, R. A. 2006, ApJ, 641, 1051
Chugai, N. N., & Danziger, I. J. 1994, MNRAS, 268, 173
De Looze, I., Barlow, M. J., Swinyard, B. M., et al. 2017, MNRAS, 465, 3309
Dwek, E., & Arendt, R. G. 2015, ApJ, 810, 75
Dwek, E., Galliano, F., & Jones, A. P. 2007, ApJ, 662, 927
Dwek, E., Sarangi, A., & Arendt, R. G. 2019, ApJL, 871, L33
Dwek, E., Staguhn, J., Arendt, R. G., et al. 2014, ApJL, 788, L30
Ercolano, B., Barlow, M. J., & Storey, P. J. 2005, MNRAS, 362, 1038
Faber, S. M., Phillips, A. C., Kibrick, R. I., et al. 2003, Proc. SPIE, 4841, 1657
Filippenko, A. V. 1997, ARA&A, 35, 309
Filippenko, A. V., & Matheson, T. 1993, IAUC, 5788, 1
Filippenko, A. V., & Matheson, T. 1994, IAUC, 5924, 1
Foreman-Mackey, D., Hogg, D. W., Lang, D., & Goodman, J. 2013, PASP, 125, 306
Fox, D. W., Lewin, W. H. G., Fabian, A., et al. 2000, MNRAS, 319, 1154
Fransson, C., Chevalier, R. A., Filippenko, A. V., et al. 2002, ApJ, 572, 350
Gall, C., Hjorth, J., Watson, D., et al. 2014, Natur, 511, 326
Garnavich, P., Challis, P., & Berlind, P. 1995, IAUC, 6174, 1
Gerardy, C. L., Fesen, R. A., Nomoto, K., et al. 2002, ApJ, 575, 1007
Gomez, H. L., Krause, O., Barlow, M. J., et al. 2012, ApJ, 760, 96
Harutyunyan, A. H., Pfahler, P., Pastorello, A., et al. 2008, A&A, 488, 383
Henning, T. 2010, ARA&A, 48, 21
Jerkstrand, A., Fransson, C., Maguire, K., et al. 2012, A&A, 546, A28
Kotak, R., Meikle, P., Pozzo, M., et al. 2006, ApJL, 651, L117
Lewin, W. H. G., Zimmermann, H. U., & Aschenbach, B. 1996, IAUC, 6445, 1
Li, W., Filippenko, A. V., Van Dyk, S. D., et al. 2002, PASP, 114, 403
Mathis, J. S., Rumpl, W., & Nordsieck, K. H. 1977, ApJ, 217, 425
Matsuura, M., Dwek, E., Barlow, M. J., et al. 2015, ApJ, 800, 50
Matsuura, M., Dwek, E., Meixner, M., et al. 2011, Sci, 333, 1258
Meikle, W. P. S., Mattila, S., Pastorello, A., et al. 2007, ApJ, 665, 608
Milisavljevic, D., & Fesen, R. A. 2008, ApJ, 677, 306
Milisavljevic, D., & Fesen, R. A. 2017, in Handbook of Supernovae, ed. A. W. Alsabti & P. Murdin (Berlin: Springer), 2211
Milisavljevic, D., Margutti, R., Kamble, A., et al. 2015, ApJ, 815, 120
Miller, J. S., & Stone, R. P. S. 1993, The Kast Double Spectograph 66, University of California Lick Observatory
Mueller, J., Brewer, C., Cappellaro, E., & della, M. 1993a, IAUC, 5784, 1
Mueller, J., Mould, J. R., & Smail, I. 1993b, IAUC, 5791, 3
Oke, J. B., Cohen, J. G., Carr, M., et al. 1995, PASP, 107, 375
Owen, P. J., & Barlow, M. J. 2015, ApJ, 801, 141
Panagia, N., Weiler, K. W., Lacey, C., et al. 2000, MmSAI, 71, 331
Pastorello, A., Aretxaga, I., Zampieri, L., Mucciarelli, P., & Benetti, S. 2005, in ASP Conf. Ser. 342, 1604-2004: Supernovae as Cosmological Lighthouses, ed. M. Turatto et al. (San Francisco, CA: ASP), 285
Pastorello, A., Benetti, S., Bufano, F., et al. 2011, AN, 332, 266
Patnaude, D., Weil, K. E., Fesen, R. A., Milisavljevic, D., & Kraft, R. P. 2025, ApJ, 980, 82
Perley, D. A. 2019, PASP, 131, 084503
Pollas, C., Albanese, D., Benetti, S., Bouchet, P., & Schwarz, H. 1995, IAUC, 6170, 1
Schaefer, B. E. 2001, IAUC, 7626, 3
Schaefer, B. E., & Roscherr, B. 1999, IAUC, 7141, 3
Shahbandeh, M., Fox, O. D., Temim, T., et al. 2025, ApJ, 985, 262
Shahbandeh, M., Sarangi, A., Temim, T., et al. 2023, MNRAS, 523, 6048
Silverman, J. M., Foley, R. J., Filippenko, A. V., et al. 2012, MNRAS, 425, 1789
Stathakis, R. A., & Sadler, E. M. 1991, MNRAS, 250, 786
Szalai, T., Fox, O. D., Arendt, R. G., et al. 2021, ApJ, 919, 17
Szalai, T., Vinkó, J., Balog, Z., et al. 2011, A&A, 527, A61
Temim, T., & Dwek, E. 2013, ApJ, 774, 8
Temim, T., Dwek, E., Arendt, R. G., et al. 2017, ApJ, 836, 129
Tinyanont, S., Fox, O. D., Shahbandeh, M., et al. 2025, ApJ, 985, 198
Turatto, M., Cappellaro, E., Danziger, I. J., et al. 1993, MNRAS, 262, 128
Van Dyk, S. D. 2013, AJ, 145, 118

Van Dyk, S. D., Sramek, R. A., Weiler, K. W., Montes, M. J., & Panagia, N. 1996, IAUC, 6386, 1
Wesson, R., Barlow, M. J., Matsuura, M., & Ercolano, B. 2015, MNRAS, 446, 2089
Wesson, R., Bevan, A. M., Barlow, M. J., et al. 2023, MNRAS, 525, 4928
Wooden, D. H., Rank, D. M., Bregman, J. D., et al. 1993, ApJS, 88, 477
Zampieri, L., Mucciarelli, P., Pastorello, A., et al. 2005, MNRAS, 364, 1419
Zsíros, S., Szalai, T., De Looze, I., et al. 2024, MNRAS, 529, 155